IEEE Access
Multidisciplinary | Rapid Review | Open Access Journal

Received September 1, 2019, accepted September 18, 2019, date of publication September 30, 2019, date of current version May 8, 2020.

Digital Object Identifier 10.1109/ACCESS.2019.2944635

Design and Test of a High-Speed Double-Winding High Temperature Superconducting Synchronous Motor

CAO JIWEI, (Member, IEEE), HAN ZHENGNAN, SONG YUCHEN, AND LI LIYI, (Senior Member, IEEE)
Harbin Institute of Technology, Harbin 150001, China

Corresponding author: Li Liyi (liliyi.hit@gmail.com)

This work was supported in part by the National Natural Science Foundation under Grant 51877053.

ABSTRACT The current carrying ability of the high temperature superconducting (HTS) material would be seriously influenced by the additional complex magnetic field. Because of this effect, the HTS material cannot be adapted in the field of high speed motors that work with high frequency current and strong magnetic field density. Therefore, this paper presents a novel HTS high speed motor system with high efficiency, high power density and high speed that could be adopted in the field of flywheel energy storage and high efficiency propulsion system. The one armature winding of the novel HTS high speed motor system is the superconducting coils, and the other armature winding is copper winding. Under this configuration, the motor with two armature windings is the doubly-fed motor. The two kinds of windings should operate in synchronous state. In this paper, a 2kW, 12000r/min high speed flywheel energy storage motor is designed. Surface magnetic field distribution of the superconducting winding and the characteristic of this type motor are detailed analyzed based on the current carrying ability of the HTS material. The new configuration of our novel HTS motor broaden the application of HTS materials in various electrical fields.

INDEX TERMS Superconducting coils, high-temperature superconductors, permanent magnet motors, critical current density, electromagnetic modeling.

I. INTRODUCTION

With the growing shortage of energy, the demand of high efficiency energy is becoming urgent. The main methods of increasing energy efficiency are decreasing the energy loss in energy transmission and use processes. Triggered by the application of superconducting technology in motors, the improvement of energy efficiency is becoming more promising.

Superconductor has the character of zero resistance and Meissner effect at low temperatures, and the application of HTS material in motor systems could realize high efficiency and high power density that has become a research focus on application of superconducting technology [1], [2].

At present, superconductor material has been mainly applied in the field of DC motors or motors with low-speed and low-frequency due to the limitation of the current carrying ability of superconductors. However, the application of HTS materials in motors with high-speed are needing more efforts [3]–[9].

As for the high power density motor system, there are two ways to increase the power density. One way is to increase the motor's torque in the unit volume. In the past decades, the superconducting motor has been adopted the superconducting coils as the rotor excitation magnetic field coils to increase the air flux density that could improve the motor torque in unit volume. The other method is to increase the speed of motor. While, high speed would lead to high frequency current and high frequency magnetic field in the motor. The high frequency current and magnetic field would decrease the current carrying ability of superconducting coils in the motor, and lead to quench of superconducting coils [10]–[13]. So, the adopting of HTS material in the high speed motor is still challenging.

This paper presented a novel high speed HTS doubly fed motor to break the limitation of the application of

The associate editor coordinating the review of this manuscript and approving it for publication was Jinquan Xu.

superconducting coil in n high frequency magnetic field. Based on characters of doubly-fed motor's, the motor adopts the superconducting winding to produce high torque and the copper winding to produce high frequency magnetic field. Moreover, ferromagnetic material is adopted to decrease the magnetic field on the superconducting coils surface. This structure can acquire both high torque and high speed to increase the motor's power density.

II. THERY OF HIGH SPEED DOUBLY-FED MOTOR SYSTEM

A. OPERATION THEORY OF DOUBLY-FED MOTOR

The doubly-fed motor has a novel motor structure that presented in the 1980s, the motor has two kinds of three-phase windings, one is the main winding known as power winding whose pole is $2p_{\mathrm{p}}$; the other winding is secondary winding known as control winding whose pole is $2p_{\mathrm{q}}$. Theoretically, these two kinds of windings have no direct electromagnetic coupling. Special structure of rotor realize the control of air magnetic field, whose pole is p_{r}. The p_{r} equals to $p_{\mathrm{p}} + p_{\mathrm{q}}$.

The two kinds of winding carry the different frequency current as shown in (1) and (2).

$$\begin{cases} i_{pA} = \sqrt{2} i_p \cos \omega_p t \\ i_{pB} = \sqrt{2} i_p \cos(\omega_p t - \frac{2}{3}\pi) \\ i_{pC} = \sqrt{2} i_p \cos(\omega_p t + \frac{2}{3}\pi) \end{cases} \tag{1}$$

$$\begin{cases} i_{qA} = \sqrt{2} i_q \cos \omega_q t \\ i_{qB} = \sqrt{2} i_q \cos(\omega_q t - \frac{2}{3}\pi) \\ i_{qC} = \sqrt{2} i_q \cos(\omega_q t + \frac{2}{3}\pi) \end{cases} \tag{2}$$

Then, the fundamental magnetic force of one phase is shown in (3) and (4).

$$\begin{cases} f_{pA1} = F_{p1} \cos \omega_p t \cos p\varphi \\ f_{pB1} = F_{p1} \cos(\omega_p t - \frac{2}{3}\pi) \cos(p\varphi - \frac{2}{3}\pi) \\ f_{pC1} = F_{p1} \cos(\omega_p t + \frac{2}{3}\pi) \cos(p\varphi + \frac{2}{3}\pi) \end{cases} \tag{3}$$

$$\begin{cases} f_{qA1} = F_{q1} \cos \omega_q t \cos q\varphi \\ f_{qB1} = F_{q1} \cos(\omega_q t - \frac{2}{3}\pi) \cos(q\varphi - \frac{2}{3}\pi + \alpha) \\ f_{qC1} = F_{q1} \cos(\omega_q t + \frac{2}{3}\pi) \cos(q\varphi + \frac{2}{3}\pi + \alpha) \end{cases} \tag{4}$$

where, α is the included angle between the magnetic forces of the two kinds of winding, F_{p1} and F_{q1} are magnetic force amplitude value of these two windings respectively.

N_{p} and N_{q} respectively are the number of per phase series turns of main and secondary winding, k_{pw1} and k_{qw1} respectively are the fundamental winding coefficient of main and secondary winding.

$$F_{p1} = \frac{4}{\pi} \frac{\sqrt{2}}{2} \frac{N_p k_{pw1}}{p} I_p \tag{5}$$

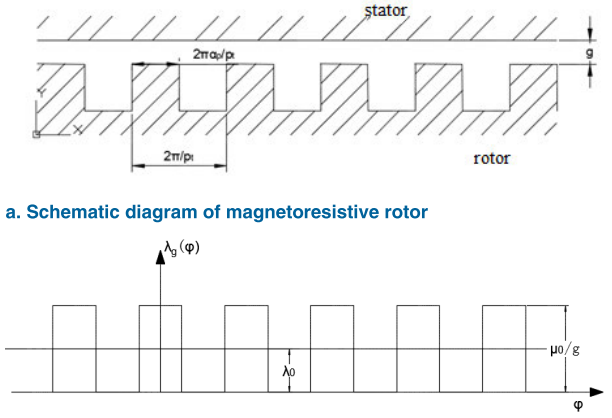

a. Schematic diagram of magnetoresistive rotor

b. Air-gap relative specific permeance function of ideal reluctance rotor

FIGURE 1. Reluctance motor schematic diagram and specific permeance function.

$$F_{q1} = \frac{4}{\pi} \frac{\sqrt{2}}{2} \frac{N_q k_{qw1}}{q} I_q \tag{6}$$

The winding fundamental synthetic magnetic force amplitude is shown as the (7) and (8):

$$f_p(\varphi, t) = F_{pm} \cos(\omega_p t - p\varphi) \tag{7}$$

$$f_q(\varphi, t) = F_{qm} \cos(\omega_q t - q\varphi + \alpha) \tag{8}$$

where, ψ is the mechanical angle relative to the stator reference coordinate.

The three-phase winding fundamental magnetic motive force (MMF) of the two kinds of the winding are respectively shown as (9) and (10).

$$F_{pm} = \frac{3}{2} \frac{4}{\pi} \frac{\sqrt{2}}{2} \frac{N_p k_{pw1}}{p} I_p \tag{9}$$

$$F_{qm} = \frac{3}{2} \frac{4}{\pi} \frac{\sqrt{2}}{2} \frac{N_q k_{qw1}}{p} I_q \tag{10}$$

It can be seen from Fig.1 that magnetic resistance rotor has ideal magnetic resistance characteristic taken no account of the effect of cogging torque and magnetic potential in ferromagnetic material. As shown in Fig.1, air magnetic conductivity is zero between teeth, and air magnetic conductivity is constant value on the top of the teeth.

It is assumed that the number of rotor tooth is *P*r, the arc coefficient is α_{p}, the air length is g at the top of teeth. When the rotor is fixed, the air-gap magnetic conductivity function is shown as (11).

$$\lambda_g(\varphi) = \lambda_0 + \sum_{\nu=1}^{\infty} \lambda_\nu \cos \nu\, p_r(\varphi - \theta_{r0}) \tag{11}$$

where, λ_0 is the average value of the air-gap magnetic conductivity, λ_ν is the amplitude value of the ν order harmonic of magnetic conductivity, θ_{r0} is the angle between the rotor reference and magnetic potential axis of the main winding.

The reference [1] described that the value of first harmonic of the magnetic field is maximum, so the high-order harmonics could be ignored, and the air-gap specific magnetic conductivity function is shown in (12).

$$\lambda_g(\varphi) = \lambda_0 + \lambda_1 \cos p_r(\varphi - \theta_{r0}) \tag{12}$$

where,

$$\lambda_0 = \alpha_p \frac{\mu_0}{g} \tag{13}$$

$$\lambda_1 = 2(\frac{\sin(\alpha_p \pi)}{\pi})\frac{\mu_0}{g} \tag{14}$$

When the speed of the rotor is ω_{rm}, the air-gap specific magnetic conductivity function is shown as (15).

$$\lambda_g(\varphi) = \lambda_0 + \lambda_1 \cos[p_r(\varphi - \theta_{r0} - \omega_{rm} t)] \tag{15}$$

Then, the air-gap flux density can be described in (16).

$$B(\varphi, t) = [f_p(\varphi, t) + f_q(\varphi, t)]\lambda_g(\varphi, t) \tag{16}$$

Equation (16) can be rewritten as (17) with (7), (8) and (15) brought into.

$$B(\varphi, t) = B_{p0} + B_{q0} + B_{p1(+)} + B_{p1(-)} + B_{q1(+)} + B_{q1(-)} \tag{17}$$

where,

$$B_{p0} = F_{pm}\lambda_0 \cos(p\varphi - \omega_p t) \tag{18}$$

$$B_{q0} = F_{qm}\lambda_0 \cos(q\varphi - \omega_q t) \tag{19}$$

$$B_{p1(+)} = F_{pm}(\lambda_1/2) \cos[(p + p_r)\varphi - (\omega_p + p_r\omega_{rm})t - p_r\theta_{r0}] \tag{20}$$

$$B_{p1(-)} = F_{pm}(\lambda_1/2) \cos[(p - p_r)\varphi - (\omega_p - p_r\omega_{rm})t - p_r\theta_{r0}] \tag{21}$$

$$B_{q1(+)} = F_{qm}(\lambda_1/2) \cos[(q + p_r)\varphi - (\omega_q + p_r\omega_{rm})t - \alpha - p_r\theta_{r0}] \tag{22}$$

$$B_{q1(-)} = F_{qm}(\lambda_1/2) \cos[(q - p_r)\varphi - (\omega_q - p_r\omega_{rm})t - \alpha - p_r\theta_{r0}] \tag{23}$$

It can be seen from the equation (15) that by modulating stator winding MMF, six kinds of magnetic field with different frequency are produced in the air-gap. Based on the theory of motor, the electromechanical conversion will be realized when the frequency of the winding current is equal to that of the air-gap flux density. In the six kinds of the flux density described by the equation (15), B_{p0} and B_{q0} are the pulsation magnetic field which cannot produce back EMF and torque; then, when p, q and p_{r} are adapted the specific value, the frequency of the last four kinds of magnetic field can be equal to the frequency of the winding current.

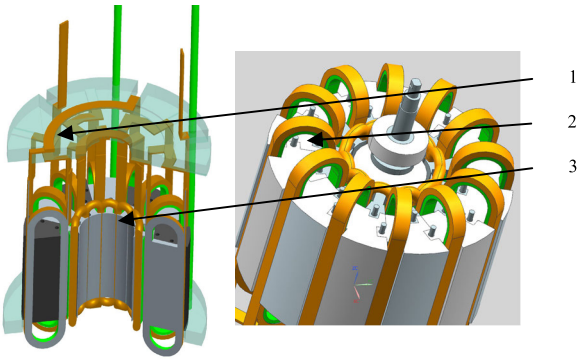

FIGURE 2. Schematic diagram of the high speed HTS motor. (1 is the current lead; 2 is the superconducting coil; 3 is the copper coil).

B. OPERATION THEORY OF DOUBLY-FED HTS MOTOR

Based on the theory of doubly-fed motor, the HTS wire is adapted in the doubly-fed motor. So, the motor has two kinds of winding which are located in stator slots, and the copper winding produces high frequency magnetic field with small current, the superconducting winding produces low frequency magnetic field with large current. The two kinds of winding output torque together to reach the optimized result.

The structure of the high speed HTS motor is shown in figure.2. The HTS wire is winded into racetrack type coils. Then it can be located in the stator slots because the superconducting coils should only be made in the mould. While, the end of the copper winding cannot connect with the superconducting winding for decreasing the influence of high frequency on the superconducting winding. Therefore, the superconducting winding adapts back round structure and the copper winding adapt traditional structure. Then two kinds of winding present a radial orientation. Copper winding constructs quadrupole winding arrangement structure ($p = 2$), superconducting winding constructs dipole winding arrangement structure ($q = 1$), the rotor constructs 6 poles magnetic barrier type structure ($p_{\mathrm{r}} = p + q = 3$). The quadrupole magnetic field in stator is induced by dipole magnetic field through modulation effect of rotor magnetic pole, and the fundamental and harmonic wave produced by the quadrupole winding are belong to even order harmonic wave for the dipole winding, those harmonic wave cannot produce effective electric potential. So the harmonic wave, in superconducting winding (dipole winding) would be smaller that would improve the superconductor wire's current carrying ability. When the motor is running, the two kinds of winding would output torque together with super synchronous mode.

When the motor speed is $\omega_{\mathrm{rm}} = [(\omega_{\mathrm{p}} + \omega_{\mathrm{q}})/(p + q)]$, the magnetic field produced by the superconducting winding and copper winding are respectively shown as:

$$B_{p1(-)} = F_{pm}(\lambda_1/2) \cos(\omega_q t - \varphi - 3\theta_{r0}) \tag{24}$$

$$B_{q1(-)} = F_{qm}(\lambda_1/2) \cos(\omega_p t - 2\varphi - \alpha - 3\theta_{r0}) \tag{25}$$

where, $B_{\mathrm{p1(-)}}$ is the magnetic field produced by the superconducting winding, and ω_{q} is its angular frequency; $B_{\mathrm{q1(-)}}$ is the

TABLE 1. High speed HTS motor design objective.

Item	Value
Power	10 kW
Rate Speed	12000 r/min
Max Speed	13000 r/min
Rate Voltage	380 V
Superconductor	ST-05-EL/200[a]

[a]ST-05-EL/200 superconductor is produced by Shanghai Superconductor with critical current 200A.

magnetic field produced by the copper winding, and ω_p is its angular frequency.

Meanwhile, the induced voltage frequency of the superconducting and copper winding is the same with their respective current frequency, then the superconducting winding and copper winding simultaneously output their electromagnetic power.

Moreover, the air-gap flux density also contains other harmonic flux density as shown in (28) and (29).

$$B_{p1+} = F_{pm}(\lambda_1/2)\cos[(2\omega_p + \omega_q)t - 5\varphi + 3\theta_{r0}] \quad (26)$$

$$B_{q1+} = F_{qm}(\lambda_1/2)\cos[(2\omega_p + \omega_q)t - 4\varphi + \alpha + 3\theta_{r0}] \quad (27)$$

It can be seen that, the air-gap flux density function not only has the $B_{p1(-)}$ and $B_{q1(-)}$ respective to dipole and quadrupole magnetic field, but also has the harmonic flux density whose frequency is $2\omega_p + \omega_q$. In addition, the two kinds of winding also produce their pulse flux density in air-gap.

III. DESIGN OF THE DOUBLY-FED HIGH SPEED HTS MOTOR

A. DESIGN OF THE DOUBLY-FED HIGH SPEED HTS MOTOR

Based on the above theory, this paper presents a novel 2kW/12000rpm high speed HTS motor, and its design objective is shown in table 1.

The table 2 gives the motor's parameters, those parameters are optimized by FEM software.

The FEM model is established using the parameters in table 2, as shown in Fig.3.

When the motor starts, the superconducting winding carries DC current whose max value is 60 A, meanwhile, the copper winding carries AC current whose frequency is 600 Hz and effective value is 4 A. The motor is running in start mode.

It can be seen from the Fig.4 and Fig.5 that the high speed HTS motor start torque is 1.79 Nm, and the output power reach 2.25 kW which is produced by the copper winding.

When the superconducting winding carries AC current (maximum value is 60A, frequency is 50Hz), the high speed HTS motor speed would be improved from 12000 rpm to 13000 rpm, then the motor is running in super-synchronous mode, the superconducting winding and the copper winding

TABLE 2. High speed HTS motor structure parameter.

Item	Value
Out Diameter of Stator	160 mm
Inner Diameter of Stator	60 mm
Iron Length	100 mm
Poles and Slots	4p-12s (copper winding) 2p-12s (superconducting winding)
Turn Number of Superconducting Winding	16
Turn Number of Copper Winding	120
Current of Superconducting Winding	80 A (DC current) /60 A (AC current)
Current of Copper Winding	4 A
Current Frequency of Superconducting Winding	DC / 50 Hz
Current Frequency of Copper Winding	600 Hz
Slot Type of Copper Winding	Flat Slot
Slot Type of Superconducting Winding	Rectangular Slot
Slot Open Width	1 mm
Slot Open Height	0.5 mm
Slot Height of Copper Winding	10 mm
Slot Height of Superconducting Winding	10 mm
Slot Width of Superconducting Winding	14 mm
Structure of Superconducting coil	Double cake type coil[a]
Width of Superconducting Winding	8 mm
Height of Superconducting Winding	10 mm

[a] Double cake type coil mean that the two coils' inner leading-wire are connected, so the coils' leading-wire are located on the lateralis of the coils as shown in fig.3.

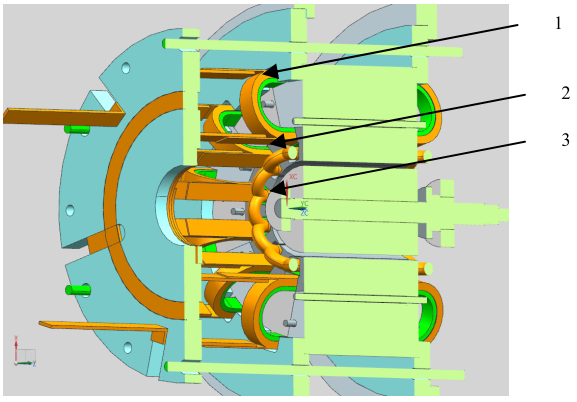

FIGURE 3. High speed HTS motor FEM simulation model (1 is the superconducting coil; 2 is the copper coil; 3 is the rotor).

together output mechanical torque, the motor's power will be improved.

It can be seen from Fig.6 that when the superconducting winding carries AC current the superconducting winding output mechanical power through the magnetic field modulation effect. The output torque of the motor improves from

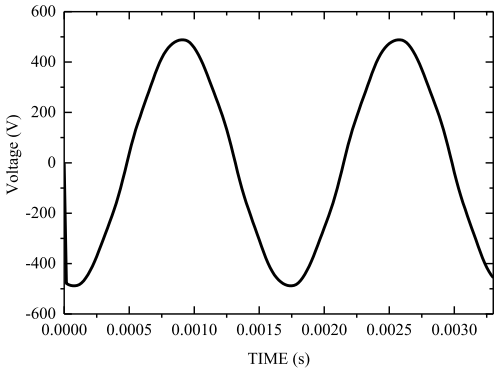

FIGURE 4. High speed HTS motor copper winding back EEF wave when the motor is running in start mode.

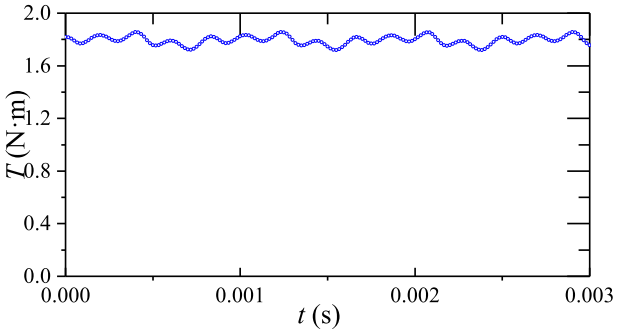

FIGURE 5. High speed HTS motor start torque curve.

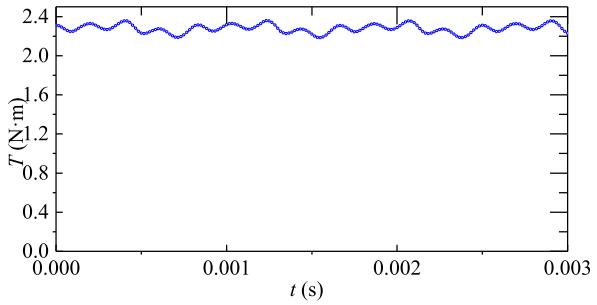

FIGURE 6. HTS motor output torque curve in super-synchronous mode (the superconducting winding carries 60 A, 50 Hz current).

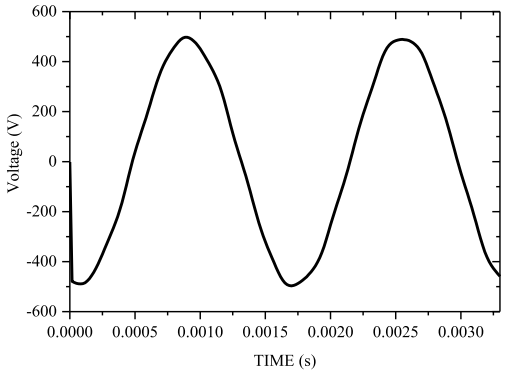

FIGURE 7. The copper winding back EEF curve when the motor is running in super-synchronous mode.

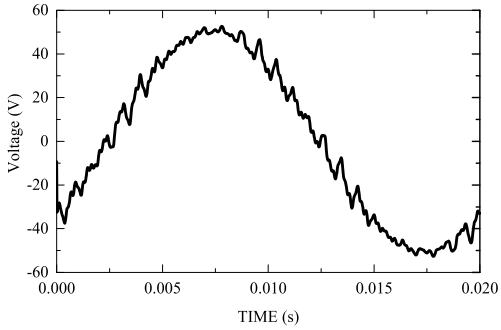

a. The superconducting winding back EEF curve.

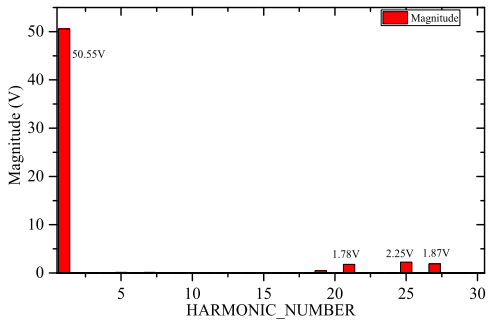

b. FFT analysis of the superconducting winding back EEF curve.

FIGURE 8. The superconducting winding back EEF curve when the motor is running in super-synchronous mode.

1.79 Nm to 2.3 Nm, and the speed improves from 12000 rpm to 13000 rpm, so the output power improves from 2.25 kW to 3.13 kW, the power increased is electromagnetic power of the superconducting winding.

The back EMF of the superconducting winding and copper winding can be seen from Fig.7 and Fig.8.

It can be seen from Fig.7 and Fig.8 that the frequency of back EMF in superconducting winding is the same with the frequency of the current. The copper winding maintains the original power output capacity. So the two kinds of winding could output electrical power to the motor. But it can be seen from Fig.8b that in the superconducting winding there is not only the foundational back EMF with the frequency of 50 Hz, but also 21 order, 25 order and 27 order harmonic wave of back EEF with high frequency. The fundamental harmonic frequency is 50Hz, and its back EMF amplitude value is 50.55 V, and the other harmonic back EMF amplitude are 1.78 V(21 order 1050Hz), 2.25V(25 order 1250Hz) and 1.87V(27 order 1350Hz). Those harmonic wave are produced by stator teeth and the magnetic field with different frequency are produced in the air-gap as shown in (17).

B. ANALYSIS OF MAGNETIC FIELD ON THE SUPERCONDUCTING WINDING SURFACE IN START MODE

When the motor is running in super synchronous mode, the superconducting winding and copper winding respectively

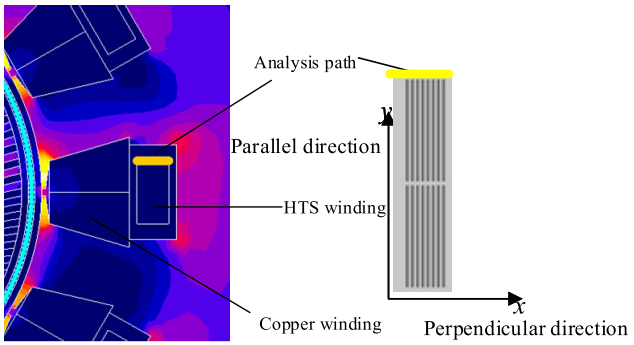

FIGURE 9. Diagram of magnetic field in slot of HTS motor.

carry current with different frequency and produce magnetic field with different frequency. Through the magnetic field modulation effect of the magnetic barrier rotor, the magnetic flux of one winding links that of another winding. Because of the limit of superconductor current carrying ability by the additional magnetic field, this paper analyzes the magnetic field distribution on the superconducting winding surface.

As shown in Figure 9, the x direction is the motor radius direction, and the yellow line is the magnetic field distribution analysis path.

When the motor is running in start mode, the superconducting winding carries DC current, and the copper winding carries high frequency AC current. Therefore, through the FEM calculation, the parallel magnetic field and perpendicular magnetic field on the HTS winding surface are respectively shown in Fig.10(a) and Fig. 10(b).

It can be seen from Fig. 10(a) and 10(b) that when the motor running in start mode the maximum flux density of parallel magnetic field is 81 mT, and the value of parallel magnetic field is decreasing along the slot height orientation. The maximum value of the perpendicular magnetic field is 35 mT, and the maximum value occurs at the middle position of superconducting coils. The reason is that the perpendicular component of the slot leakage magnetic field is generated by the superconducting coils and reaches maximum on the middle position, the magnetic field vector on the both side would be attracted by the iron material to became parallel component.

Meanwhile, the superconducting winding also work under the parallel magnetic field. During the one period, the parallel magnetic field on the superconducting winding surface is shown as Fig. 11.

It can be seen from the Fig.11 that the superconducting winding surface magnetic field could be divided into two kinds, one is the steady magnetic field that is produced by the superconducting winding and its maximum value is 78.09 mT, the other is the alternating magnetic field that produced by copper winding and its maximum value is 1.75 mT.

Fig. 12 describes the perpendicular magnetic field on the superconducting coil surface. It can be seen from the Fig. 12a and Fig. 10b, the perpendicular magnetic field maximum

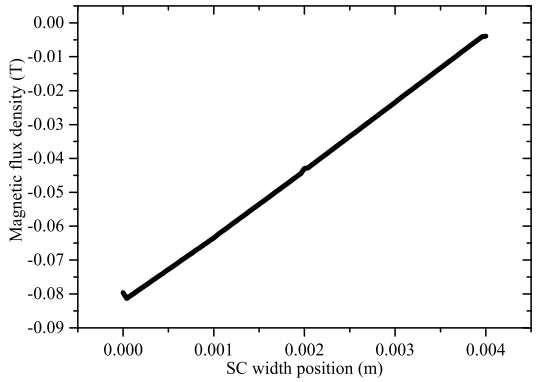

a. Parallel magnetic field distribution on the superconducting winding surface.

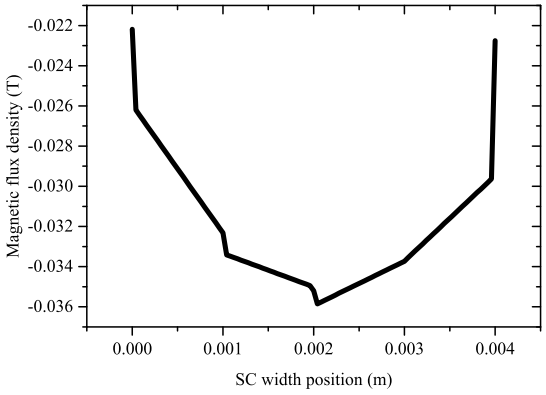

b. Perpendicular magnetic field distribution on the superconducting winding.

FIGURE 10. The magnetic field distribution on the superconducting winding surface.

value occurs in the middle of the superconducting coil. Therefore, the middle point (width is 2 mm) is analyzed for obtaining the magnetic field distribution and frequency, as shown in Fig. 12b and Fig. 12c. The amplitude and frequency of magnetic field distribution.

It can be seen from Fig. 12b that when the motor is working in starting state, the magnetic field on the superconducting winding is the steady magnetic field produced by the superconducting current, and its maximum value is 35 mT. the high frequency magnetic field maximum value is only 0.78 mT produced by the copper winding.

It can be seen from Fig. 11 and Fig.12 that though the copper winding carries the high-frequency current, the high-frequency magnetic field value on the superconducting winding is little, and the magnetic field on superconducting winding is mainly steady magnetic field produced by the direct current carried by superconducting coils.

C. ANALYSIS OF MAGNETIC FIELD ON THE SUPERCONDUCTING WINDING SURFACE IN SYNCHRONOUS MODE

When the motor is running in super synchronous mode, the magnetic field on the superconducting coils is shown in Fig.13.

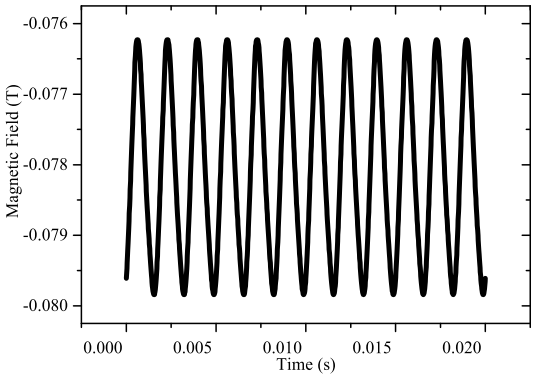

a. Parallel magnetic field of the one point on the superconducting winding (superconducting coils(SC) width =0 mm) with time.

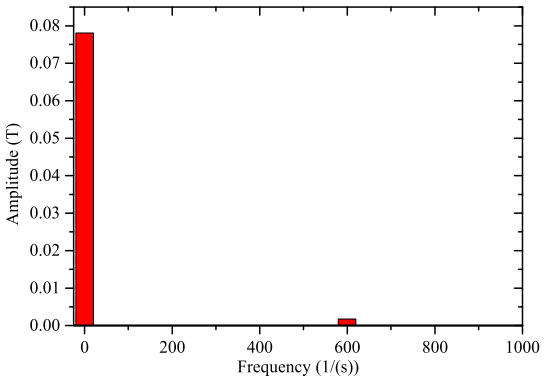

b. FFT result of the parallel magnetic field on the one point (sc width =0 mm.

FIGURE 11. Parallel magnetic field distribution on superconducting winding surface.

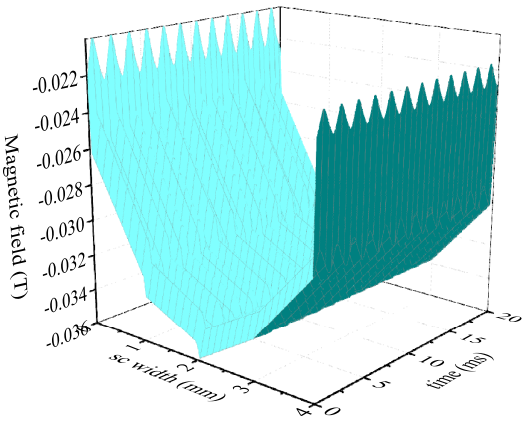

a. Perpendicular magnetic field on the superconducting with time.

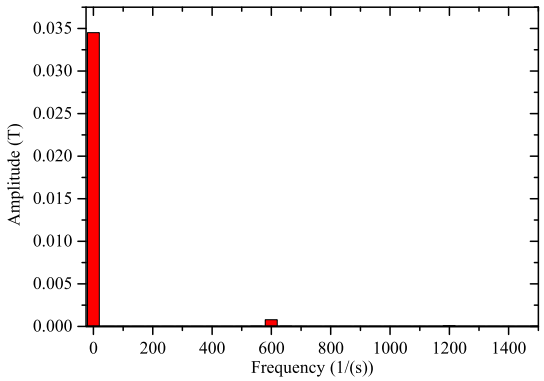

b. FFT result of the perpendicular magnetic field on the one point (sc width =0 mm).

FIGURE 12. Perpendicular magnetic field distribution on supercon-ducting winding surface.

It can be seen from Fig.13 that when the motor is running in super synchronous mode, the maximum value of perpendicular magnetic field on the superconducting coil surface is 81 mT, and the maximum value of parallel magnetic field is 35 mT. Compared with starting mode, there are no difference between them. The result is that the iron core attracts the magnetic field and its flux density is not saturation.

It can be seen from Fig. 13a and Fig.14a that the parallel magnetic field value varies obviously with the spatial position, and the maximum value occurs in the position close to the copper winding. Therefore, the point (sc width=0 mm) is analyzed for its value and frequency. Fig. 14c describe time-dependent curve of magnetic field on this point. The parallel magnetic field has two kinds of frequency, one frequency is the same with the frequency of the current carried by superconducting coils, and the maximum value of magnetic field is 78.15 mT. The other is the same with the frequency of current carried by copper coils, and its maximum value of magnetic field is 1.67 mT. The result proves that the parallel magnetic field on the superconducting coil is produced by superconducting winding, the magnetic field produced by copper winding has little influence on the superconducting coils.

Meanwhile, the perpendicular magnetic field distribution on the superconducting coil surface is shown in Fig.15.

It can be seen from Fig. 15 that the perpendicular magnetic field frequency is also the same with the frequency of current carried by superconducting coils. Though the current carried by the copper winding also produces the magnetic field on the superconducting coils, its amplitude is small. The result proves that the perpendicular magnetic field on the superconducting coil is mainly produced by superconducting winding, the high frequency magnetic field produced by the copper winding has little effect on the superconducting coil.

Compared between the Fig. 14 and Fig. 15, when the motor is running in super synchronous mode, magnetic field on the superconducting coils surface is mainly produced by its current, the high frequency magnetic field produced by the copper winding current is small. From the FFT result of parallel and perpendicular magnetic field, high frequency magnetic field only accounts less than 2.6% of low frequency magnetic field.

IV. HTS COILS WINDING AND PROTOTYPE TESTING

The core of high speed HTS motor is the superconducting material. Therefore, the characteristic of the HTS tape

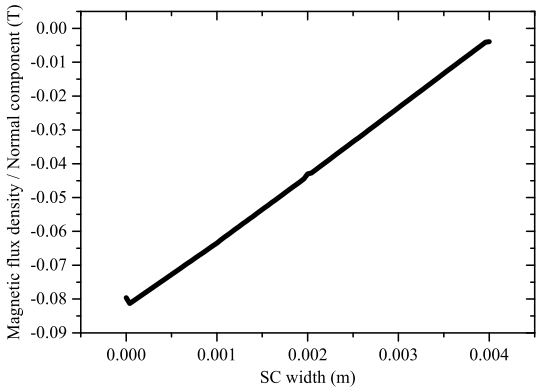

a. Parallel magnetic field distribution on the superconducting winding (0.02s).

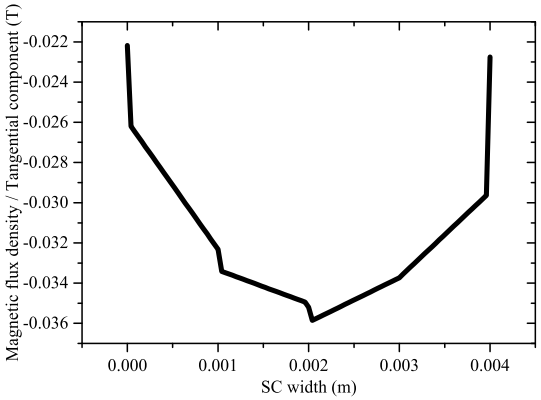

b. Perpendicular magnetic field distribution on the superconducting winding (0.02s).

FIGURE 13. Magnetic field distribution on the superconducting winding in super synchronous mode.

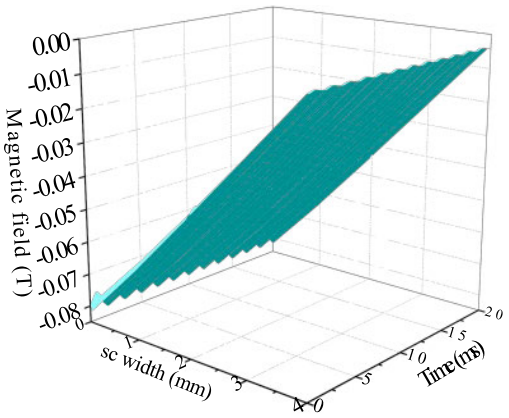

a. Parallel magnetic field distribution curve with time.

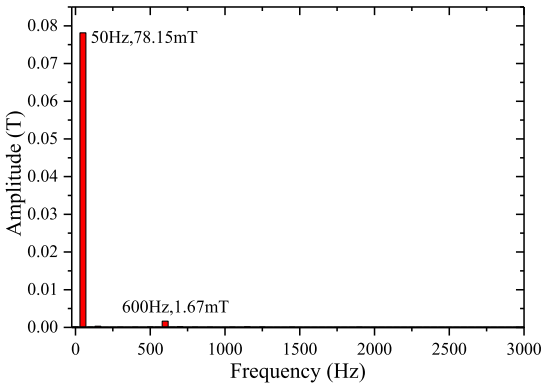

b. FFT result of parallel magnetic field on the point (sc width =0 mm).

FIGURE 14. Parallel magnetic field distribution with time.

ST-05-EL/200 is tested firstly. The carrying ability of this material is tested to supply the theoretical basis for the HTS high speed motor design.

Based on the motor design, the current in the superconducting winding would not be larger than 60 A, which could ensure the reliability and safety because the current is less than critical current.

So, the double-cake race-track coils are winded, and the turn number of the coil is fourteen.

The critical current of the HTS coil shown in Fig. 16 is tested. The critical current curve is tested under self-field as shown in Fig.17a. The critical current curve is tested under 0.03T AC magnetic field as shown in Fig.17b.

It can be seen from Fig.17a that the critical current of double-pancake HTS coil is 150 A. HTS motor's superconducting winding only need the HTS coils could carry 60A current, so the coil could meet the motor. And form the Fig.17b, under the AC magnetic field 0.03T, the critical current could be 200A with magnetic field frequency of 300Hz. Meanwhile, the critical current could be larger than that under AC magnetic field of higher frequency because of the superconductor wire's substrate materials.

Based on the analysis, the prototype motor is manufactured as shown in Fig. 18.

As shown in Fig. 18, the motor outermost shell is the vacuum container, which is adapted as the thermal insulation. And the vacuum container could be divided into two parts, one is the adapted as the thermal insulation, and the other is adapted as vacuum chamber which locates the motor shaft, as shown in Fig. 19.

The superconducting coils as well as copper coils are immersed in liquid nitrogen. In order to provide cool ability of liquid nitrogen, this paper analyzes energy loss throughout the entire system: copper loss, superconductor AC loss, and the iron loss. From equation (28) and (29), the thermal loss of superconducting coils and copper coils could be calculated as [10]–[12].

$$P_{per} = 4\mu_0 a^2 J_c H_c d[\frac{\beta}{2}\ln(\cosh\beta) - \tanh\beta] \cdot S \cdot l \cdot f \quad (28)$$

$$P_{cu} = I^2 R = 15^2 \times 0.22 = 49.5\text{W} \quad (29)$$

where, a is the half length of the superconducting tape; i is the normalized current and is defined as I_a/I_c where I_a is the transport-current amplitude, I_c is the critical current; β is defined as B_a/B_p where B_p is the penetration field at

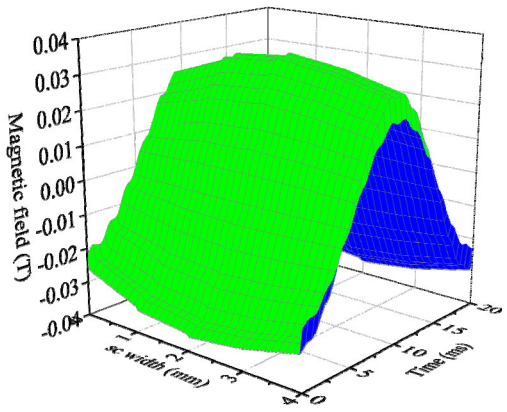

a. Perpendicular magnetic field distribution curve with time.

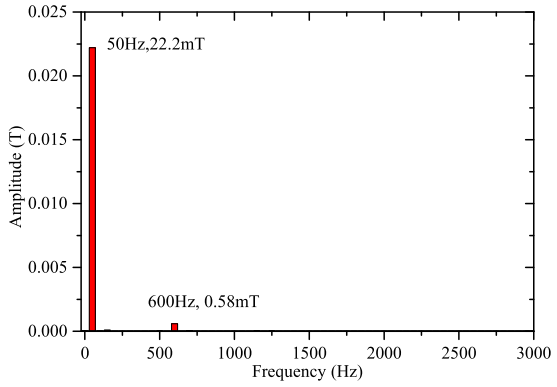

b. FFT result of perpendicular magnetic field on the point (sc width =0 mm).

FIGURE 15. Perpendicular magnetic field distribution with time.

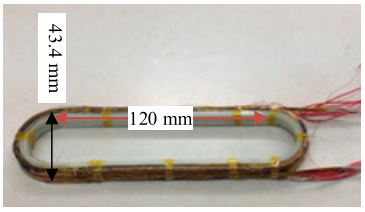

FIGURE 16. Winded HTS coil.

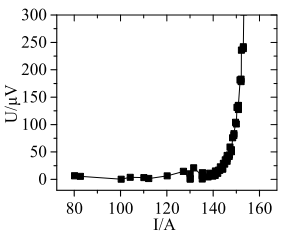

a. Double-cake HTS coil critical current curve with no magnetic field.

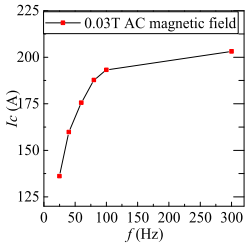

b. Double-cake HTS coil critical current curve with 0.03T AC magnetic field.

FIGURE 17. Double-cake HTS coil critical current curve.

zero transport current, B_a is the amplitude of magnetic field; S is the section area of the superconducting tapes; f is the

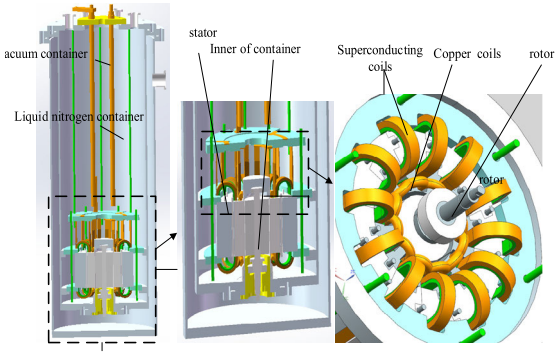

FIGURE 18. High-speed HTS motor 3D sketch.

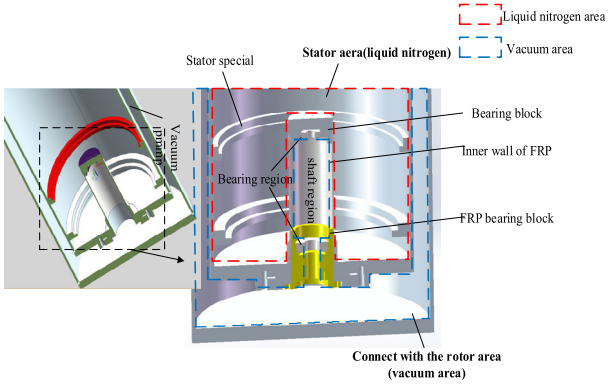

FIGURE 19. Vacuum container 3D sketch.

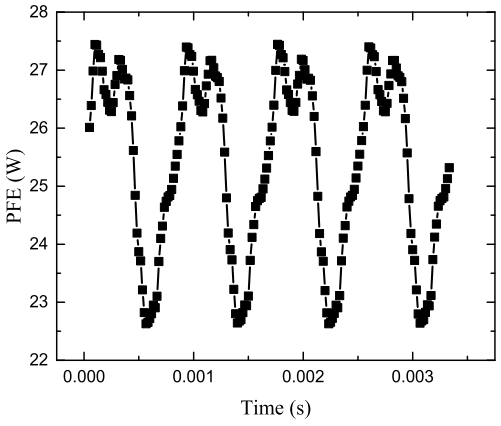

FIGURE 20. Iron loss with a period.

frequency of the current;l is the coils' length. And the thermal loss of superconducting coil is 1.52W.

Then, the iron loss is calculated by FEM software as shown in figure.20.

It could be seen from the figure.20 that the iron loss is 25 W when the motor is in super-synchronous mode. So, the total loss in the high speed motor is 76.074 W.

From equation (28) and (27), the thermal loss in liquid nitrogen could be absorbed by gasification of liquid nitrogen at 77K.

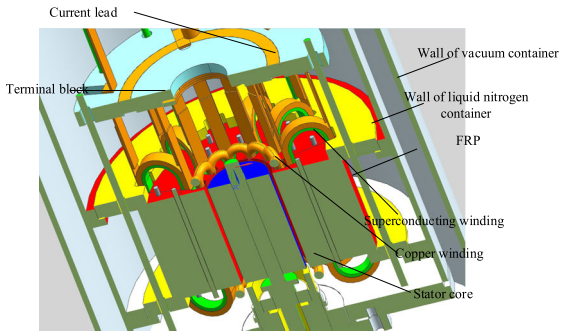

a. stator structure sketch.

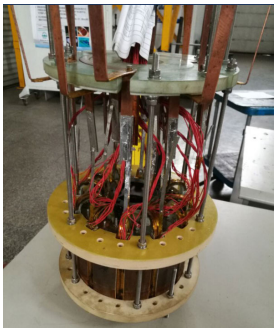

b. photo of the stator.

FIGURE 21. High-speed HTS motor stator core sketch.

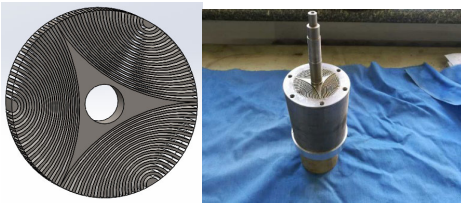

FIGURE 22. HTS motor rotor and shaft.

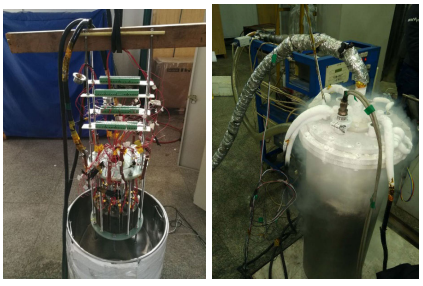

FIGURE 23. HTS motor prototype.

For ensuring the safety of copper winding, the copper coils are adapted with epoxy encapsulation. The superconducting coils are winded to race-track coils and located in the separation core. The separation cores are connected with the dovetail groove located on the epoxy encapsulation copper winding as shown in Fig. 21.

The rotor is adapted as the ALA magnetic barrier rotor as shown in Fig. 22.

So the prototype is manufactured as shown in Fig. 23.

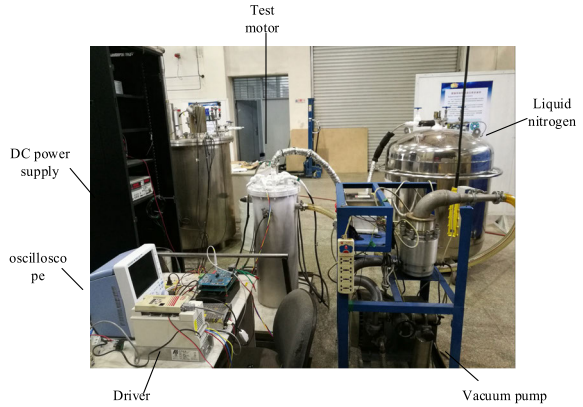

FIGURE 24. Test site picture.

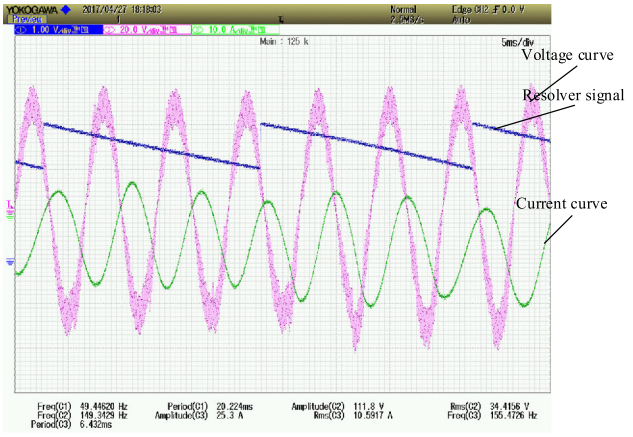

FIGURE 25. Current, line voltage and position signal of the HTS motor (3000r/min).

This motor is tested for getting the back EMF and the speed. The KEB driver is adapted to control current of the copper winding, and the Agilent 6681A power is adapted to supply the current of the superconducting winding. The test principle is shown in Fig. 24.

The DC power supply output 60A to the superconducting winding, and the driver controlled the speed from 1000 r/min to 3000 r/min. Fig.25 shows the motor current curve (green line), the copper winding line voltage curve (pink line) and the resolver signal curve (blue line) when the copper winding current frequency is 150 Hz. From the resolver signal, the motor speed is 3000 r/min, this result is consistent with the design result.

When the motor is running at the speed of 1000 r/min, the switch is disconnected, and then the copper winding back EMF can be tested. As shown in Fig. 24, when the switch is disconnected, the first peak-to-peak value of the copper winding line voltage is 77.4V, that could be the copper winding back EMF value. And the back EMF coefficient is 0.774 V/Hz, it is consistent with the design result.

The speed is adjusted, and the different back EMF is tested as shown in Fig.26. When the speed is below 2000 r/min, the back EMF coefficient is stable; when the speed is beyond 2000 r/min, the back EMF coefficient becomes small,

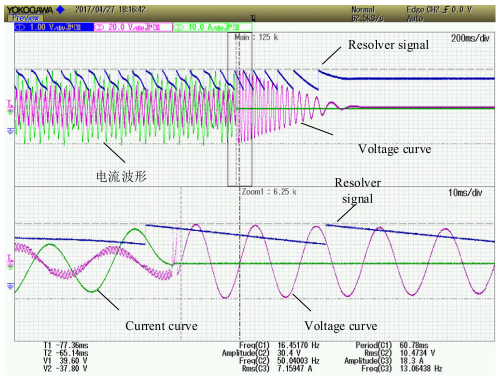

FIGURE 26. Back-EMF measurement of the motor (1000r/min).

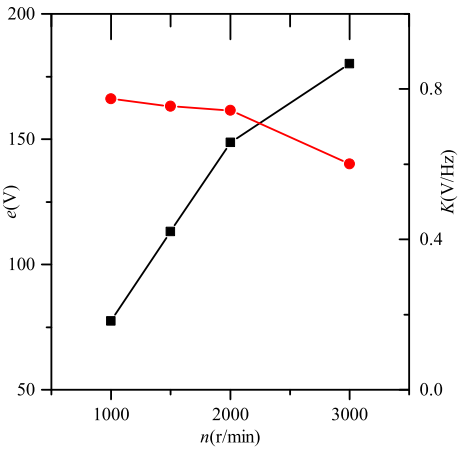

FIGURE 27. Back-EMF and Back-EMF coefficient at different speed of the motor (the red line is the back EMF coefficient and the black line is the back EMF).

TABLE 3. High speed HTS motor winding critical current.

Phase	Connect Number	Critical Current [a]
A phase	1-2-8-7	145 A
A phase	9-10-4-3	145 A
A phase and B phase	1-2-8-7-12-6-5	145 A
A phase and C phase	1-2-8-7-9-10-4-3	145 A

[a] the test is running with no magnetic field environment.

the reason is that when the shaft is 3000r/min, the rotor emerges whirling because of bearing clearance. The bearing clearance is caused by the low temperature of liquid nitrogen, and the motor running noise become larger.

When the motor speed is 3000 r/min, the superconducting winding critical current is tested as shown in table 3.

From table 3, the different connect mode cannot influence the superconducting winding critical current. The critical current is 145A, it could ensure the HTS motor running reliably.

V. CONCLUSION

This paper presents a novel double winding high speed HTS motor to solve the difficult problems of superconductor application, such as the limitation of bending radius influenced by strong and high-frequency magnetic field, low AC current carrying ability as well as seldom application of superconductor in motors with small volume and high speed. The novel HTS motor adapted copper winding and superconducting winding to obtain high-speed and high power density. This paper analyzes the starting character, performance of steady state and the coupling relation between the superconducting winding and the copper winding of this HTS motor. The simulation of operating curves, analysis of magnetic field and the related experiments prove the possibility of the high-speed double windings HTS motors. The prototype motor with high-speed double windings is designed and fabricated, and the test of superconducting coil prove the feasibility of superconducting coil to apply in high-speed motors.

We will further test this prototype motor to investigate the limitation of current carrying ability and operation frequency and the feasibility of the application of HTS materials in high-speed motors.

REFERENCES

[1] C. A. Luongo, P. J. Masson, T. Nam, D. Mavris, H. D. Kim, G. V. Brown, M. Waters, and D. Hall, "Next generation more-electric aircraft: A potential application for HTS superconductors," *IEEE Trans. Appl. Supercond.*, vol. 19, no. 3, pp. 1055–1068, Jun. 2009. doi: 10.1109/TASC.2009.2019021.

[2] P. J. Masson, J. E. Pienkos, and C. A. Luongo, "Scaling up of HTS motor based on trapped flux and flux concentration for large aircraft propulsion," *IEEE Trans. Appl. Supercond.*, vol. 17, no. 2, pp. 1579–1582, Jun. 2007. doi: 10.1109/TASC.2007.898111.

[3] G. Snitchler, B. Gamble, and S. S. Kalsi, "The performance of a 5 MW high temperature superconductor ship propulsion motor," *IEEE Trans. Appl. Supercond.*, vol. 15, no. 2, pp. 2206–2209, Jun. 2005. doi: 10.1109/TASC.2005.849613.

[4] B. Gamble, G. Snitchler, and T. MacDonald, "Full power test of a 36.5 MW HTS propulsion motor," *IEEE Trans. Appl. Supercond.*, vol. 21, no. 3, pp. 1083–1088, Jun. 2011. doi: 10.1109/TASC.2010.2093854.

[5] M. Frank, J. Frauenhofer, P. van Hasselt, W. Nick, H.-W. Neumueller, and G. Nerowski, "Long-term operational experience with first siemens 400 kW HTS machine in diverse configurations," *IEEE Trans. Appl. Supercond.*, vol. 13, no. 2, pp. 2120–2123, Jun. 2003. doi: 10.1109/TASC.2003.813013.

[6] G. Nerowski, J. Frauenhofer, G. Ries, W. Nick, and H.-W. Neumiiller, "Advances and prospects of HTS rotating machine development at Siemens," in *Proc. IEEE Power Eng. Soc. Gen. Meeting*, Denver, CO, USA, Jun. 2004, pp. 2052–2055.

[7] S. K. Baik, Y. K. Kwon, H. M. Kim, J. D. Lee, Y. C. Kim, and G. S. Park, "Electrical performance analysis of HTS synchronous motor based on 3D FEM," *Phys. C, Supercond. Appl.*, vol. 470, no. 20, pp. 1763–1767, Nov. 2010. doi: 10.1016/j.physc.2010.05.202.

[8] S. K. Baik, M. H. Sohn, E. Y. Lee, Y. K. Kwon, T. S. Moon, H. J. Park, and Y. C. Kim, "Effect of synchronous reactance and power factor on hts synchronous machine design and performance," *IEEE Trans. Appl. Supercond.*, vol. 16, no. 2, pp. 1489–1492, Jun. 2006. doi: 10.1109/TASC.2005.864460.

[9] M. Iwakuma, A. Tomioka, M. Konno, Y. Hase, T. Satou, Y. Iijima, T. Saitoh, Y. Yamada, T. Izumi, and Y. Shiohara, "Development of a 15 kW motor with a fixed YBCO superconducting field winding," *IEEE Trans. Appl. Supercond.*, vol. 17, no. 2, pp. 1607–1610, Jun. 2007. doi: 10.1109/TASC.2007.898480.

[10] W. T. Norris, "Calculation of hysteresis losses in hard superconductors carrying ac: Isolated conductors and edges of thin sheets," *J. Phys. D, Appl. Phys.*, vol. 3, no. 4, pp. 489–507, May 2002. doi: 10.1088/0022-3727/3/4/308.

[11] N. Amemiya, N. Enomoto, and S. Shirai, "FEM analysis of AC loss in twisted Bi-2223 multifilamentary tapes carrying AC transport current in AC transverse magnetic field with arbitrary orientation," *IEEE Trans. Appl. Supercond.*, vol. 14, no. 2, pp. 782–785, Jun. 2004. doi: 10.1109/TASC.2004.830269.

[12] W. Yuan, M. D. Ainslie, W. Xian, Z. Hong, Y. Chen, Y. Yan, R. Pei, and T. A. Coombs, "Theoretical and experimental studies on J_c and AC losses of 2G HTS coils," *IEEE Trans. Appl. Supercond.*, vol. 21, no. 3, pp. 2441–2444, Jul. 2011. doi: 10.1109/TASC.2010.2088366.
[13] X. Li, S. Yu, and Y. Wang, "A novel HTS claw-pole vernier machine using single excitation unit with stationary seal," *IEEE Trans. Appl. Supercond.*, vol. 29, no. 5, Aug. 2019, Art. no. 5201505. doi: 10.1109/TASC.2019.2895567.

CAO JIWEI (M'19) was born in Harbin, Heilongjiang, China, in 1983. He received the B.S. and M.S. degrees in electrical engineering from the Shenyang University of Technology, in 2005 and 2008, respectively, and the Ph.D. degree in electrical engineering from the Harbin Institute of Technology, in 2014.

Since 2014, he has been a Research Assistant with the Electrical Engineering Department, Harbin Institute of Technology. He holds 15 patents. His research interests include high power density permanent magnets motors, high-temperature superconducting motors, high-speed motors, and motors measurement technology.

Dr. Cao was a recipient of the Science and Technology Progress of Ministry of Education, in 2011, and the International Conference on Electric and Intelligent Vehicles Best Paper Award, in 2018.

HAN ZHENGNAN was born in Harbin, Heilongjiang, China, in 1985. He received the B.S., M.S., and Ph.D. degrees in electrical engineering from the Harbin Institute of Technology, China, in 2009, 2011, and 2017, respectively.

From 2017 to 2019, he was a Research Assistant with the Space Basic Science Research Center, Harbin Institute of Technology. His research interests include high temperature superconducting motor technology and accelerator magnet technology.

SONG YUCHEN was born in Daqing, Heilongjiang, China, in 1996. He received the B.S. degree in electrical engineering from the Harbin Institute of Technology, Harbin, China, in July 2017, where he is currently pursuing the Ph.D. degree in electrical engineering.

From 2017 to 2019, he was a Ph.D. Postgraduate with the Electrical Engineering Department, Harbin Institute of Technology. His research interests include optimization, analysis, and design of high-speed motors.

LI LIYI (M'11–SM'18) received the B.E., M.E., and D.E. degrees from the Harbin Institute of Technology (HIT), Harbin, China, in 1991, 1995, and 2001, respectively.

Since 2004, he has been a Professor with the School of Electrical Engineering and Automation, HIT, where he became a "Yangtze Fund Scholar" Distinguished Professor, in 2013. He is currently supported by the National Science Fund for Distinguished Young Scholars. He has authored or coauthored more than 110 technical articles and holds 50 patents. His research interests include design, drive and control of linear motors, and design and drive of high-speed/power density permanent magnet machines.